J Mater Sci: Mater Med (2008) 19:1349–1354
DOI 10.1007/s10856-007-3164-9

Self-assembly and bioactive response of a crystalline metal oxide in a simulated blood fluid

Robert Lynn Karlinsey · Keewook Yi

Received: 30 January 2006 / Accepted: 14 September 2006 / Published online: 4 October 2007

Abstract In this study we report on the bioactive response of self-assembled niobium oxide microstructures when immersed in a supersaturated solution emulating mineral content in blood. The structures were formed via electrochemical anodization in an electrolyte comprised of HF and NaF. The slow oxide formation kinetics associated with the presence of NaF in the electrolyte enabled microscopic examinations during microstructure evolution as shown via scanning electron microscopy (SEM). Apparently the slow growth kinetics encourage the development of bioactive sites on the microstructures, as these structures induced mineral formations. On the other hand, microstructures grown in the absence of salt were ineffective mineral nucleators. Analysis of nucleated mineral deposits was performed using X-ray diffraction and Raman spectroscopy. Both long-range and short-range order experiments verified the nucleated mineral phase was hydroxyapatite (HAP). Further characterization of the mineral phase was observed using SEM and revealed effective nucleation sites were predominantly isolated to loci on the ordered microbodies as opposed to locations lying within the amorphous strata.

R. L. Karlinsey (✉)
Department of Preventive & Community Dentistry, Oral Health Research Institute, Indiana University School of Dentistry, Indianapolis, IN 46202, USA
e-mail: rkarlins@iupui.edu

K. Yi
School of Earth and Environmental Sciences, Seoul National University, Seoul 151-747, Korea

Introduction

Apatites are important calcium phosphorous minerals comprising the major constituent in bone and teeth [1, 2]. When biological apatite in the body becomes damaged or severely weakened, synthetic options in the form of biomaterials [3, 4] are employed either as a substitution or to stimulate recovery through bond formation with the living tissue [5, 6]. Since the first documented clinical implant procedure in the 1750's [6], over 245,000 hip and knee replacements [4] and over 100,000 dental implants [7] are preformed annually in the US. This number is likely to continue to rise due to the natural aging of large and small populations as well as inherent problems associated with existing implants, such as aseptic loosening [8] and mechanical failure [9]. To help improve implant performance and functionality [9], as well as expedite bone-repair and healing times [7], advanced biomaterials exhibiting greater nucleation capability are required [10, 11]. Typically, these biomaterials embody metals [12], bioactive glass [13], glass ceramics [14], and functionalized metal oxides [11].

With respect to metal oxides, the dielectric properties and chemical stability and inertness provide for extensive applications ranging from electronic [15–17] and optical [18, 19] devices to bioactive coatings on orthopedic implant materials [11, 20]. Still new applications may evolve when metal oxides are tailored to specific geometries such as ribbons [21], tubes [22, 23], and webs [24]. And while metal oxides can be formed through various methodologies [15, 21, 24, 25], anodization offers an efficient and relatively inexpensive method of producing structured metal oxides such as titania [22] and zirconia [23] nanotubes for use as potential microanalytical tools [26], for example.

In the present study we present new details regarding the nucleation and growth of niobium oxide microcones formed in situ by electrochemical anodization in an HF electrolyte containing NaF. And, while the resulting Nb_2O_5 microcones bearing sub-micronsized tips have potential in point-source [27], sensing [28], and catalysis [29] applications, we show the ceramic also manifests biological advantages by commanding a strong bioactive response when immersed in a supersaturated solution emulating a physiological fluid. Instead of an ion-exchange process serving to nucleate mineral, a process that apparently contributes to the nucleation efficiency of Bioglass [13] and functionalized metal oxides [30], the present microstructures appear to possess meso and nanoscale nucleation sites formed through the self-assembly of crystalline microcones. Furthermore the resulting bioactivity is realized only when salt is present in the electrolyte. Therefore, details regarding the self-assembly of crystalline niobium oxide microcones demonstrated in this work provides for a simple and powerful way to develop highly structured materials with broadly impacting applications.

Experimental methods

Anodization of niobium foil

Formation of niobium oxide is described as follows. 99.8% pure niobium foil 0.25 mm thick was purchased from Aldrich and HF acid (48% assay) was obtained from Fisher Scientific. The niobium metal was rinsed with acetone and ethanol and cut into one centimeter wide strips. The acid was diluted with the appropriate amount of deionized water to achieve a concentration of 2.5 wt.% HF. The HF(aq) solutions contained NaF salt (Aldrich) ranging between 100 and 250 mg. Anodization of the niobium metal was driven by a Sorensen DLM 300-2 power supply connected to copper and niobium metal electrodes. The electrodes were positioned in a Nalgene beaker that contained 100 mL of magnetically agitated electrolyte and was maintained at 35 °C. A 20 V potential was employed to stimulate oxide development. Under these conditions changes in current were observed throughout anodization, indicating oxide rate forming processes and steady-state conditions. In an electrolyte solution containing 100 mg NaF the duration of anodization lasted up to 90 min at 35 °C. The anodized foil was then removed from the electrolyte and rinsed thoroughly with distilled water. Small squares several millimeters in size were sectioned from the niobium foil and placed aside for biomimetic studies.

Preparation of simulated body fluid

To test for bioactivity, we immersed the anodized niobium foil in a supersaturated solution based on a well-established simulated body fluid (SBF) that mirrors results from in vivo studies [31]. The ion concentrations used in this work (2.5 mM Ca^{2+}, 1.0 mM HPO_4^{3-}, 5.0 mM K^+, 1.5 mM Mg^{2+}, 150.4 mM Na^+, 153.0 mM Cl^-, 4.2 mM HCO_3^-, 0.5 mM SO_4^{2-}) emulate the content found in human blood plasma. The reagents (Fisher Scientific) used to obtain the formulation are as follows: 0.368 g $CaCl_2{\cdot}2H_2O$, 0.136 g KH_2PO_4, 0.296 g KCl, 8.307 g NaCl, 0.445 g Na_2CO_3, 0.094 g $MgCl_2$, and 0.06 g $MgSO_4$ were dissolved in 1 Lof deionized water. The fluid was buffered with trishydroxymethyl aminomethane and adjusted to a pH of 7 with HCl. The solution was stored at 4 °C for over four weeks and showed no visible signs of precipitation. Multiple 2×2 mm^2 squares were cut from the anodized foil and placed in individual vials containing 15 mL SBF, covered with parafilm and placed in an oven at 37 °C.

Characterization

Characterization of microscopic oxide and mineral morphology was performed in high vacuum mode using a JEOL JSM-5310LV scanning electron microscope (SEM).

X-ray diffraction (XRD) patterns of niobium oxide, hydroxyapatite (HAP) reference (hydroxyapatite Bio-Gel HTP Gel, Bio-Rad Laboratories), and niobium oxide immersed in the SBF were collected on a Siemens 5000 automated powder diffractometer with a 0.02° 2θ step-size operating at 40 kV/30 mA. Using Bruker EVA software, oxide patterns were fingerprinted to orthorhombic Nb_2O_5 (JCPDS card # 27-1003).

Raman spectroscopy was performed using a Raman spectrometer model T64000 (HORIBA Jobin Yvon). Spectra were generated from a 514 nm laser source impinging on the samples at an intensity of 50 mW for 50 s. For consistency, the HAP reference material examined by Raman spectroscopy was the same as that used in X-ray diffraction.

Results and discussion

We begin by discussing the development of the self-assembled bioactive ceramic. Characterization of microscopic oxide was performed using scanning electron microscopy (SEM). The progression of the resulting oxide produced by anodizing niobium foil at 20 V in an electrolyte solution comprised of 2.5 wt.% HF(a) and 100 mg

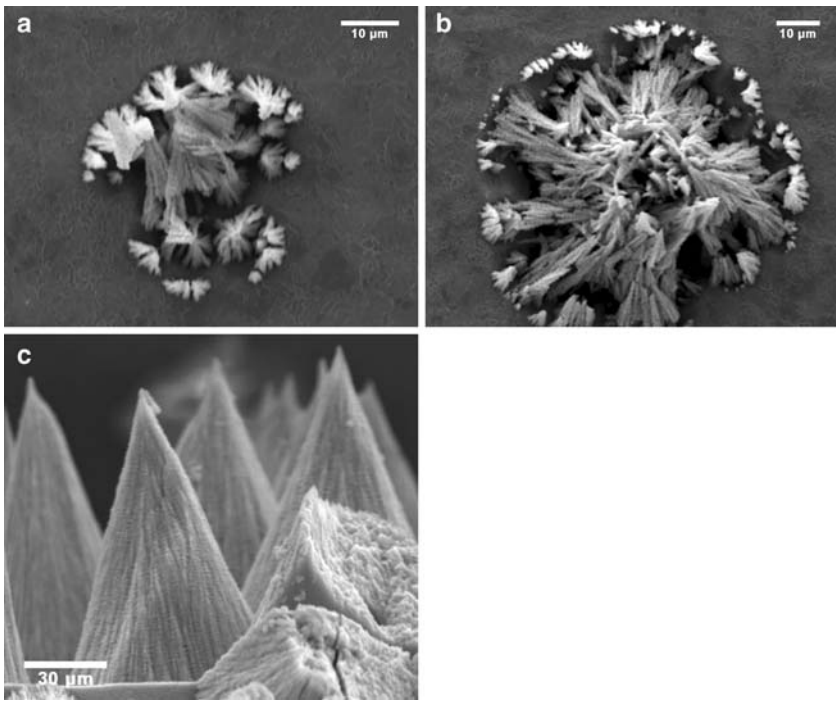

Fig. 1 Progression of ceramic microcone self-assembly. (**a**) Top view SEM image showing early self-assembly of niobium oxide fibers after 20 min anodization in 2.5 wt.% HF + 100 mg NaF solution. (**b**) Continued self-assembly driven by oxide thickness-dependent evolution of current field rings after 35 min anodization. (**c**) Densification of microcones (cross-sectional view) at steady-state after 70 min anodization

NaF is shown in the SEM images in Fig. 1. Due to rapid oxidation sourced by a constant potential, the morphology of the initial oxide phase is amorphous and is well-described by existing models [32, 33], where adsorbed water and hydroxyl anions react with interstitial niobium ions at the interface to form the new disordered phase. After some time (e.g. $\sim$ 20 min at 35 °C), however, the semblance of some ordered structure in the form of oxide fibers up to 10 μm long evolves from the amorphous oxide background as observed in Fig. 1a. The relatively high transport number of oxygen during anodization [34] suggests the evolution of these structures most likely develops from an oxygen diffusion-limited [33] secondary growth process. Since the oxide and metal are both soluble in HF(aq) [32], defects, grain boundaries and cracks in the niobium foil subsequently become more pronounced, creating wider pathways to allow interstitial ions lying within the bulk niobium foil to readily react with the faster diffusing oxygen ions [35] within the amorphous strata.

Prolonged anodization (e.g. $\sim$ 35 min at 35 °C) creates additional structures, many of which appear to converge with one another, forcing protrusions from the foil plane as shown in Fig. 1b. Comparison between Fig. 1a and b shows the ordered oxide appears to develop step-wise in concentric rings, beginning with a 'center' and gradually expanding outward. The center may be defined as high concentrations of defects and/or grain boundaries that approximate sub-micron to micronsized points [36]. The corresponding circular (due to 2-D constraints of the foil) fields, the diameter of which is modulated by amorphous oxide thickness at fixed potential, apparently stimulate structure development through promotion of mobile interstitial niobium ions within the bulk foil to the oxide surface. As both the oxide and foil thin over the anodization period due to HF dissolution, the current field strength evolves under potentiostatic conditions, becoming more extensive (i.e. additional field rings develop), thereby stimulating new self-assembly. When steady-state is attained, the rate of oxide formation approximates the dissolution rate and the field strength stops evolving. These processes are validated experimentally by monitoring current versus time. At steady-state, self-assembly continues within the range of the limited field, resulting in a time-dependent densification of microconical structures with meso and nanoscale tips like those images in the cross-sectional view Fig. 1c. Within this image the cross-sectional views of the broken structures in the lower right-hand corner further reveal microcone densification while the slightly out-of-focus structures visible within the depth-of-field suggest patterned arrays of microbodies may be produced according to both random and inflicted (e.g. by scratching, cutting, or etching the foil surface) defects. Such densification of microconical structures shown in Fig. 1c has not been realized previously for niobium oxide or other metal oxides.

Recently we have discussed the preparation conditions of fully developed self-assembled microstructures like that in Fig. 1c [37]. However, the microcones formed in this work differ markedly in several ways due to the apparent sensitivity in electrolytic conditions. For example, Nb_2O_5 crystal sizes and morphology are strongly influenced by the presence of salts (e.g. NaF or NaH_2PO_4) in the HF(aq)

electrolyte during anodization [38]. The purpose of adding salt to the electrolyte was to impart control on the self-assembly by limiting the flux of oxygen contributing to oxide formation [34, 35] through the coordination of water molecules to Na^+. Kinetically, relatively longer anodization times were required to attain microcone structures of the same size in the absence of salt, which likely bears on the long-range ordering of the oxide. As a direct result of the present work, the addition of NaF also permits an assessment into the possible mechanism of oxide nucleation and growth as discussed above and shown in Fig. 1.

The discussion regarding the presence of salt in the electrolyte during anodization has important ramifications to biological applications since microcones developed in an HF electrolyte without NaF did not exhibit bioactivity when immersed in a simulated body fluid (SBF) as shown in Fig. 2a. The lack of mineral growth may be surprising since the microcones manifest large surface area sites, defects, and coarseness, aspects that have been known to assist in mineral nucleation from supersaturated fluids. When anodized in the presence of NaF (Fig. 2b), however, the self-organized microcones heterogeneously nucleated Ca-P mineral and is a most interesting result of this work. At this point, however, we point out that X-ray energy dispersive analysis did not reveal evidence of Na incorporation into the ceramic microstructures; therefore the microstructures were not predisposed to nucleation of mineral through Na functionalization. Additional features in the Fig. 2c Nb_2O_5 XRD pattern after an eight-day immersion in SBF marks the presence of a new phase. The peaks centered about 26° and 32° were assigned to hydroxyapatite (HAP) when compared to the crystalline HAP reference pattern shown in Fig. 2d. The lattice mismatch between the Nb_2O_5 (001) (i.e. ~ 22.6°) and HAP (002) (i.e. ~ 26°) crystal faces was calculated to be as low as 1.1%. Such close lattice matching implicates epitaxy as a possible factor in the heterogeneous nucleation of HAP. The relatively broad lineshapes tentatively assigned to HAP in Fig. 2c indicate the presence of a polycrystalline phase comprised of small crystals; in order to unambiguously identify and build support for mineral assignment, the short-range order was probed using Raman spectroscopy. The Raman spectra for the HAP reference and an HAP-capped ceramic sample are presented in Fig. 3. Within the 800–1200 cm^{-1} range, the pronounced resonance near 960 cm^{-1} is characteristic of the P–O stretch in the PO_4 tetrahedra of HAP [2]. The marked coincidence of the two spectra provides strong short-range evidence for HAP assignment and corroborates the indexing from X-ray diffraction.

The SEM images in Fig. 4 reveal substantial mineral growth after eight days immersion in a physiological fluid emulating the content found in human blood plasma. Remarkably, HAP appears almost exclusively on the self-organized structures, either partially or fully covering the ceramic microbodies as shown in Fig. 4a, b. This indicates the rough, amorphous oxide layer does not embody effective HAP nucleators. These observations coupled with the dense coverage near the center of Fig. 2b where the number of nearest neighbors is high suggest the microstructures manifest multiple heterogeneous nucleation sites

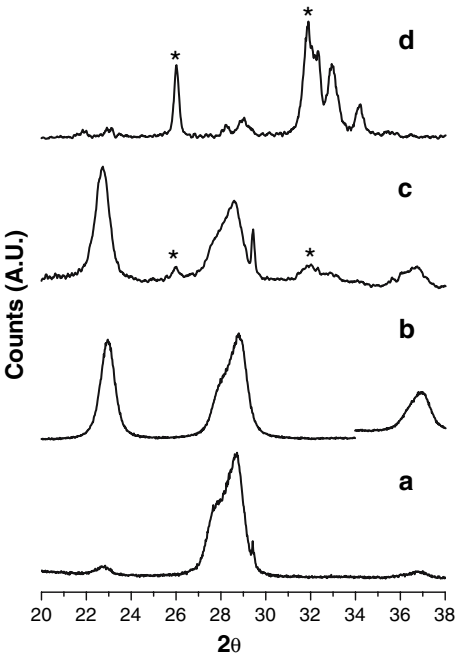

Fig. 2 X-ray diffraction patterns of Nb_2O_5 formed in the absence of NaF and immersed in the simulated body fluid (**a**), formed in the presence of NaF (**b**) and immersed in the simulated fluid (**c**), and of the HAP reference material (**d**). For clarity, asterisks are shown in (**c**, **d**) to indicate HAP near 26° and 32°

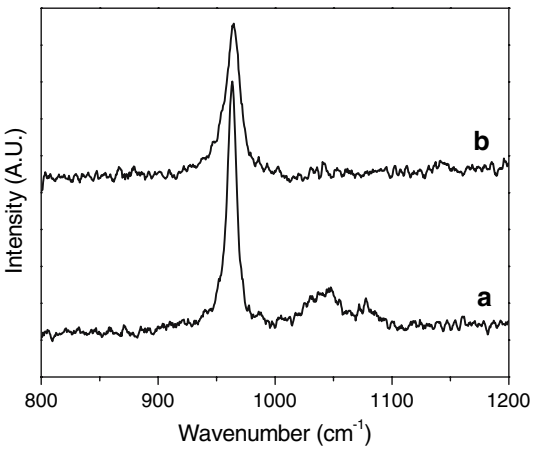

Fig. 3 Identification of mineral phase. Raman spectra of HAP reference powder (**a**) and of mineral phase nucleated on Nb_2O_5 ceramic after immersion in SBF for eight days (**b**). The vibrational response centered 960 cm^{-1} confirms presence of HAP

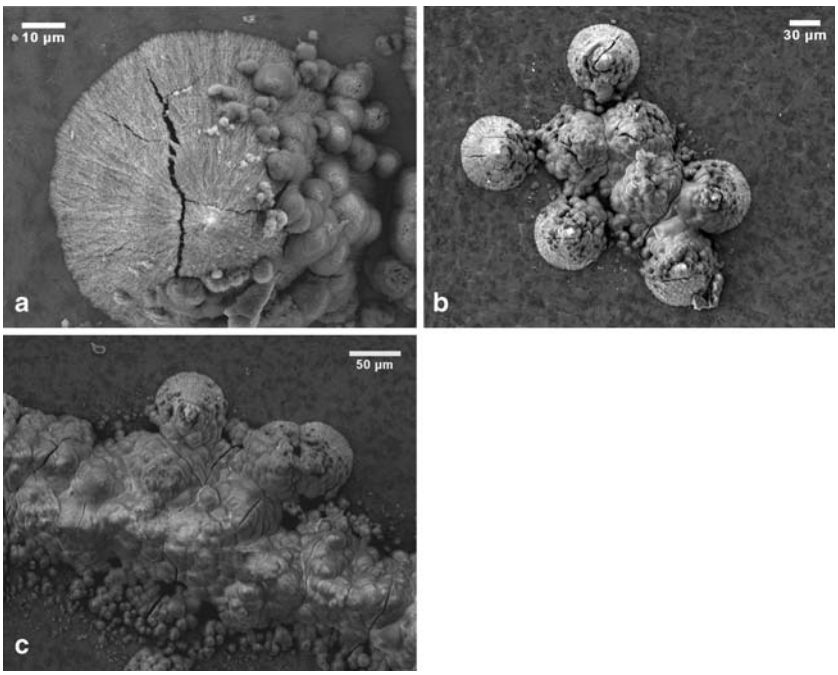

Fig. 4 Bioactive response of self-assembled microcones in SBF. SEM images of self-assembled ceramic showing exclusivity of HAP nucleation to microcones (**a**, **b**) and extent of HAP formation when microcones evolve in close proximity (**c**)

as shown in Fig. 4a. The quality of the site, however, is likely modulated by the self-assembly process shown in Fig. 1. The relatively sparse mineral development on the microcones away from the center suggests the importance of connectivity and is further supported in Fig. 4c: beneath the extensive mineral layer, the underlying ceramic terrain can be described as a microscopic mountain range. Again it is obvious that the visible amorphous strata near the top of the image bear no indication of potential primary nucleation sites. The impressive HAP coverage blanketing the 200 µm-long ceramic chain and tapering near the coneplain edges further stresses the necessity and effectiveness of the self-assembled microbodies in primary nucleation. Such massive HAP deposits on Nb_2O_5 contrasts significantly with that formed on Biolgass [13, 39] and functionalized metal oxides [11, 30] with similar immersion times, while implicating improved tissue bonding and expedited healing times.

Here we note that HAP growth was still observed when the microcones were pulverized using a mortar and pestle and immersed in the simulated fluid; thus, the meso and nanoscale sites created through the self-assembly process presumably manifest effective nucleation centers while the microscopic conical geometry does not appear critical for mineral nucleation. Additionally, when microcones were formed in the absence of NaF, apparently the rapid self-assembly precluded the development of effective nucleation sites, as no HAP nucleation was observed. These observations underline the sensitivity and influence of the self-assembly process on material properties, such as bioactivity, at the meso and nanoscales.

Conclusion

In conclusion, we presented insight into the nucleation and growth of Nb_2O_5 microstructures in an HF electrolyte containing NaF formed via electrochemical anodization. Interestingly, microstructures formed in the absence of salt did not effectuate mineral nucleation. Apparently, the controlled growth produces effective nucleation sites at the meso and nanoscales and may be related to the self-assembled arrangement of Nb_2O_5 crystals during anodization, a possbility we are currently investigating. Regardless of the mechanism, however, this is the first time a non-functionalized, highly ordered metal oxide has nucleated mineral from a simulated fluid emulating the mineral content found in blood. These results may bear on the future development of innovative biomaterials.

Acknowledgments Support for this study was funded by the Oral Health Research Institute. The authors thank Ms. Y.H. Cho at National Center for Inter-University Research Facilities at Seoul National University for assistance and use of the Raman spectrometer. The authors also thank Dr. Jeffrey Swope and Mr. Vince Hernly at IUPUI for assistance with X-ray diffraction. The authors are grateful to A.T. Hara for valuable discussions and give special thanks to Clif W. Duhn for assistance with image processing.

References

1. A. S. POSNER, *Physiol. Rev.* **49** (1969) 760
2. B. WOPENKA and J. D. PASTERIS, *Mat. Sci. Eng. C* **25** (2005) 131

3. L. L. HENCH and J. WILSON, In *An Introduction To Bioceramics*, edited by. L. L. Hench and J. Wilson (New Jersey, World Scientific: 1993) p.1
4. S. V. Bhat, *Biomaterials*, (Harrow, Alpha Science International, Ltd., 2005)
5. L. L. HENCH and J. WILSON, *Science* **226** (1984) 630
6. R. K. WOO, D. D. JENKINS and R. S. GRECO, In *Nanoscale Technology in Biological Systems*, edited by R. S. Greco, F. B. Prinz and R. L. Smith (Boca Raton, CRC Press, 2005), p 1
7. D. A. PULEO and A. NANCI, *Biomaterials* **20** (1999) 2311
8. P. H. WOOLEY and E. M. SCHWARZ, *Gene. Ther.* **11** (2004) 402
9. A. GRATTON, B. BUFORD, T. GOSWAMI, D. GADDYKURTEN and L. SUVA, *J. Mech. Behav. Mater.* **13** (2002) 297
10. L. C. CHOW, *Adv. Dent. Res.* **2** (1988) 181
11. T. KOKUBO, H.-M. KIM and M. KAWASHITA, *Biomaterials* **24** (2003) 2161
12. M. UCHIDA, H.-M. KIM, F. MIYAJI, T. KOKUBO and T. NAKAMURA, *Biomaterials* **23** (2002) 313
13. L. L. HENCH and O. ANDERSSON, In *An Introduction To Bioceramics*, edited by L. L. Hench and Wilson J (New Jersey, World Scientific, 1993) p. 41
14. R. XIN, Y. LENG, J. CHEN and Q. ZHANG, *Biomaterials* **26** (2005) 6477
15. M. RISTIC, S. POPOVIC and S. MUSIC, *Mater. Lett.* **58** (2004) 2658
16. M. A. AEGERTER, M. SCHMITT and Y. GUO, *Int. J. Photoenergy* **4** (2002) 1
17. H. CHOOSUWAN, R. GUO and A. S. BHALLA, *Mater. Lett.* **54** (2002) 269
18. B. OREL, U. O. KRASOVEC, M. MACEK, F. SVEGL and U. L. STANGAR, *Sol. Energ. Mat. Sol. C* **56** (1999) 343
19. H. SIM, D. CHOI, D. LEE, M. HASAN, C. B. SAMANTARAY and H. HWANG, *Microelectron. Eng.* **80** (2005) 260
20. D. VELTEN, E. EISENBARTH, N. SCHANNE and J. BREME, *J. Mater. Sci-Mater. M* **15** (2004) 457
21. K. HONG, W. YIU, H. WU, J. GAO and M. XIE, *Nanotechnology* **16** (2005) 1608
22. D. GONG, C. A. GRIMES, O. K. VARGHESE, W. HU, R. S. SINGH, Z. CHEN and E. C. DICKEY, *J. Mater. Res.* **16** (2001) 3331
23. W. J. LEE and W. H. SMYRL, *Electrochem. Solid. St.* **8** (2005) B7
24. D. P. BRENNAN, A. DOBLEY, P. J. SIDERIS and S. R. J. OLIVER, *Langmuir* **21** (2005) 11994
25. H. MASUDA and K. FUKUDA, *Science* **268** (1995) 1466
26. G. K. MOR, O. K. VARGHESE, M. PAULOSE, N. MUKHERJEE and C. A. GRIMES, *J. Mater. Res.* **18** (2003) 2588
27. W. T. CHU, H. H. LIN, Y. H. WANG, C. T. HSIEH, Y. T. LIN and C. S. WANG, *IEEE Electr. Device. L* **26** (2005) 670
28. U. OZERDEM and A. R. HARGENS, *Microvas. Res.* **70** (2005) 116
29. J. HAAHEIM, R. EBY, M. NELSON, J. FRAGALA, B. ROSNER, H. ZHANG and G. ATHAS, *Ultramicroscopy* **103** (2005) 117
30. P. LI, C. OHTSUKI, T. KOKUBO, K. NAKANISHI, N. SOGA and K. de GROOT, *J. Biomed. Mater. Res.* **28** (1994) 7
31. T. KOKUBO, H. KUSHITANI, S. SAKKA, T. KITSUGI and T. YAMAMURO, *J. Biomed. Mater. Res.* **24** (1990) 721
32. J. HALBRITTER, *Appl. Phys. A* **43** (1987) 1
33. M. GRUNDNER and J. HALBRITTER, *Surf. Sci.* **136** (1984) 144
34. J. S. L. LEACH and B. R. PEARSON, *Corros. Sci.* **28** (1988) 43
35. Q. LU, T. HASHIMOTO, P. SKELDON, G. E. THOMPSPON, H. HABAZAKI and K. SHIMIZU, *Electrochem. Solid. St.* **8** (2005) B17
36. F. KELLER, M. S. HUNTER and D. L. ROBINSON, *J. Electrochem. Soc.* **100** (1953) 411
37. R. L. KARLINSEY, *Electrochem. Commun.* **7** (2005) 1190
38. R. L. KARLINSEY, *J. Mater. Sci.* **41** (2006) 5017
39. D. C. CLUPPER, J. J. Jr. MECHOLSKY, G. P. LATORRE and D. C. GREENSPAN, *Biomaterials* **23** (2002) 2599